Neutron capture cross sections and solar abundances of ^{160,161}Dy, ^{170,171}Yb, ^{175,176}Lu, and ^{176,177}Hf for the *s*-process analysis of the radionuclide ^{176}Lu

Hermann Beer and Gerold Walter
Kernforschungszentrum Karlsruhe, Institut für Kernphysik III, D-7500 Karlsruhe, Federal Republic of Germany

R. L. Macklin
Oak Ridge National Laboratory, Oak Ridge, Tennessee 37830

P. J. Patchett
Max Planck-Institut für Chemie, D-6500 Mainz, Federal Republic of Germany

(Received 6 April 1984)

The neutron capture cross sections and solar abundances of ^{160,161}Dy, ^{170,171}Yb, ^{175,176}Lu, and ^{176,177}Hf have been measured. With this data base *s*-process studies have been carried out to determine the *s*-process neutron density and temperature and to investigate the *s*-process nucleosynthesis of the ^{176}Lu clock. From various branchings the neutron density was found to be $(0.8-1.8)\times10^8$ neutrons per cm^3 and the temperature kT to be 18—28 keV. On the basis of the present data, ^{176}Lu proved not to be applicable as a cosmic clock because of the temperature sensitivity of the ^{176}Lu half-life but can be used instead as a stellar thermometer. Constraints for the *s*-process temperature ($kT=20-28$ keV) were found to be in good agreement with the investigated branchings.

I. INTRODUCTION

The isotope ^{176}Lu is the only long-lived radioactive relic which is exclusively a product of *s*-process nucleosynthesis. Therefore, it offers a unique opportunity to measure the age of the *s*-process generated nuclei of solar system matter. In spite of the many efforts to reach this goal,[1-3] until now no unequivocal *s*-process age has been obtained. The detailed treatment of *s*-process branching and the understanding of the importance of isomeric states in this connection[4-6] had opened a new dimension for ^{176}Lu so that it finally was no longer clear whether ^{176}Lu should be considered as a cosmic clock for determining the age of chemical elements or as a stellar thermometer for measuring the temperature of the *s* process.[7] As the central problem responsible for this dilemma an isomeric state in ^{176}Lu at roughly 127 keV was recognized. It seemed impossible at that time to decide easily whether this state is unaffected by internal electromagnetic couplings to neighboring states (photoexcitations and deexcitations) or whether at least a partial change of the initial populations of the ground and isomeric states is initiated by these linkings. It was shown that this question required a detailed calculation with reliable electromagnetic transition rates especially of *K*-forbidden interband transitions which are difficult to determine experimentally.[7]

Another way to decide this question was indicated by Beer.[8] It was shown that the analysis of the branched *s*-process flowing through ^{176}Hf and ^{176}Lu allows the calculation of the effective branching factor which can be compared with the branching factor under the assumed condition that the branching is solely initiated through the population of the ^{176}Lu isomer by 30 keV neutron capture of ^{175}Lu. This comparison is a crucial check and gives insight into the real significance of ^{176}Lu. This approach to the ^{176}Lu problem requires accurate capture cross sections and solar abundances of the isobaric pair ^{176}Hf and ^{176}Lu and the same data from a stable *s*-only isotope in the vicinity. It turned out that ^{160}Dy is a suitable nucleus.[8]

The present work is a quantitative assessment of this experimental approach to the ^{176}Lu problem. Capture cross section measurements were performed with two different experimental arrangements. A selected set of samples were measured twice for cross checking. The solar abundances of ^{160}Dy, ^{176}Hf, and ^{176}Lu were determined from samples of the standard meteorite Orgueil using the isotope dilution technique. As the analysis of ^{176}Lu requires also a measure of the *s*-process neutron density and temperature, an analysis of various branchings of the synthesis path is carrried out. This analysis had to be performed as part of a general $\sigma N(A)$ calculation. The good agreement of the $\sigma N(A)$ curve with experimental points is a convincing demonstration of the correctness of the σN correlation. The ^{176}Lu problem is then treated taking into account a variety of necessary corrections. Finally, it is pointed out which quantities related to ^{176}Lu need a better assessment to improve the situation.

II. MEASUREMENTS

A. Neutron capture cross sections

The measurements were carried out at the Oak Ridge Linear Accelerator (ORELA) and at the Karlsruhe 3 MV pulsed Van de Graaff accelerator using the time-of-flight technique (TOF). ORELA was operated at a repetition rate of 800 pulses per second with an electron burst width at 15 ns full width at half maximum. The water moderated evaporation neutrons from a Ta target were collimated

and impinged on the sample to be analyzed after a flight path of 40.12 m. A ^{10}B filter (0.0269 atoms/b) served to eliminate any overlap of slow neutrons. The neutron capture events in the sample were counted via the prompt emitted capture gamma radiation with a pair of C_6F_6 liquid scintillation detectors symmetrically placed outside the neutron beam at the position of the sample. Constant background events were determined from the interval where the ^{10}B filter absorbs nearly all neutrons. The time dependent backgrounds were obtained from auxiliary runs with a ^{208}Pb sample and with no sample in the neutron beam. The measurements covered the energy range from 2.6 keV to 1 MeV.

At the Van de Graaff Accelerator neutrons were produced via the ^{7}Li(p,n) reaction. The machine was run with a repetition rate of 500 kHz and a pulse width of 1.2 ns. Seven samples mounted on a multiple position sample changer were moved successively into the collimated neutron beam at a flight path distance of 0.6 m. At this position the prompt emitted gamma radiation was counted by a pair of C_6D_6 liquid scintillation detectors. The cycle period of the sample changer was monitored by a ^{6}Li glass neutron detector. The seven samples consisted of four isotopes to be investigated, a gold reference sample, a graphite sample (0.008 688 atoms/b), and an empty sample position. The empty sample position and the carbon sample were used to correct for the background events. The carbon sample served to take into account the effect of sample scattered neutrons.

The experimental parameters of the ORELA and the Van de Graaff measurements were quite different. This is demonstrated in Table I. More details of the ORELA and Van de Graaff arrangements can be found elsewhere (Beer and Macklin,[9] and references therein, and Almeida and Käppeler,[10] and references therein).

The capture events were accumulated as a function of pulse height and time of flight. In order to derive the total capture cross section the recorded pulse height must be independent of the details of the gamma-ray cascade. This is achieved by pulse height weighting the observed gamma events. This procedure results in an efficiency of the detectors which is proportional to the excitation energy (binding energy + kinetic energy) released from the deexcitation of the compound nucleus. The background subtracted capture events $C(I)$ were multiplied with the weighting function $W(I)$ and summed over the pulse height channels I. The resulting quantity is related to the isotopic capture cross sections σ_j of the sample by the following expression:

$$\sum_I C(I)W(I) \sim \phi N \cdot \mathrm{MS} \cdot K_\gamma \sum_j \sigma_j H_j E_j^* \qquad (1)$$

with excitation energy

$$E_j^* = E_{Bj} + E_n \frac{A}{A+1} ,$$

ϕ denotes the neutron flux, N the number of target nuclei, MS the corrections for neutron multiple scattering and self-shielding, and K_γ the correction for gamma-ray absorption in the sample. H_j designates the abundance of isotope j, E_{Bj} designates the respective neutron binding energy, E_n is the neutron kinetic energy, and A the target mass number. The weighting function $W(I)$ is chosen so that the detector efficiency is proportional to the excitation energy E^*. This leads to the following relation:

$$\sum_i \sum_I S(E_{\gamma i}, I)W(I) \sim \sum_i E_{\gamma i} \sim E^* . \qquad (2)$$

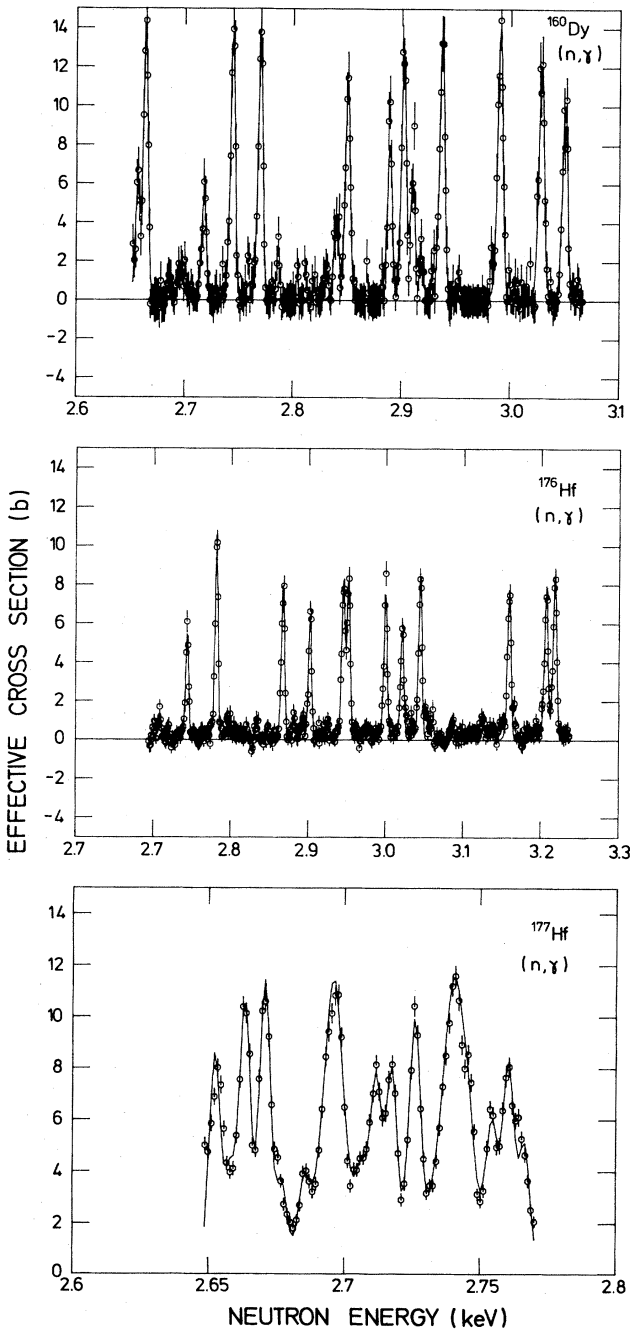

FIG. 1. Samples of ^{160}Dy(n,γ) and ^{176,177}Hf(n,γ) yield data. The solid line is generated from the least squares fitting program LSFIT (Ref. 15) to extract resonance parameters. The fit is performed including Doppler broadening, resonance self-protection, multiple scattering, and both Gaussian and exponential resolution functions.

TABLE I. Experimental parameters.

Quantity	ORELA	Van de Graaff
Neutron reaction	Neutron evaporation	^{7}Li(p,n)^{7}Be
Repetition rate	800 Hz	500 KHz
Pulse width	15 ns	1.2 ns
Flight path	40 m	0.6 m
Setup	Neutron collimators and filters C_6F_6 liquid scintillation detectors	Neutron collimators C_6D_6 liquid scintillation detectors
Flux determination	Saturated resonance technique ^{6}Li(n,α) cross section	^{197}Au(n,γ) cross section
Analysis	Weighting technique Different codes for data handling and calculation of multiple scattering and γ self-absorption	Weighting technique

The function S is the probability of obtaining a signal in channel I for the detected photon of energy $E_{\gamma i}$. The summation i is carried out over the gamma-ray cascade of the capture event.

The Van de Graaff measurements were performed relative to ^{197}Au as a standard. The gold sample was a metallic disc of 15 mm ϕ and a weight of 1.7073 g. The gold measurement combined with the gold capture cross sec-

TABLE II. Sample characteristics.

Sample	Total weight (g)	Isotopic composition (%)	Chemical composition	Dimensions (mm)
^{160}Dy	1.4681	(156) < 0.1 (158) < 0.1 (160) 69.50(161) 17.83 (162) 6.45(163) 3.55 (164) 2.67	Dy_2O_3	15ϕ×1.56
^{161}Dy	1.1359	(156) < 0.05(158) < 0.05 (160) 0.64(161) 90.41 (162) 6.52(163) 1.45 (164) 0.98	Dy_2O_3	15ϕ×1.25
^{170}Yb	1.6965	(168) 0.02(170) 78.78 (171) 10.54(172) 4.85 (173) 2.08(174) 3.05 (176) 0.68	Yb_2O_3	15ϕ×1.64
^{171}Yb	2.2731	(168) < 0.01(170) < 0.38 (171) 95.07(172) 2.61 (173) 0.74(174) 0.99 (176) 0.21	Yb_2O_3	15ϕ×2.15
^{175}Lu	1.9748	Natural	Lu_2O_3	15ϕ×1.75
^{176}Lu	2.0068	(175) 27.54(176) 72.46	Lu_2O_3	15ϕ×1.83
^{176}Hf	3.8642	(176) 64.16(177) 16.06 (178) 9.10(179) 3.41 (180) 7.27	Metal	26.6×25.3×0.6
^{177}Hf	10.327	(176) 0.86(177) 91.05 (178) 5.17(179) 1.04 (180) 1.88	HfO_2	26×52×1.65

tion substitutes for the flux and absolute efficiency indicated in Eq. (1).

In the ORELA measurements the detection efficiency is normalized by means of the saturated resonance technique using the 4.9 eV resonance of ^{197}Au.[11] As $\Gamma_\gamma \gg \Gamma_n$ for this resonance, the observed saturated capture yield near the peak (sample thickness 0.0029 atoms/b) is proportional to the incident neutron flux because virtually all (97.7%) of the neutrons are captured. The energy dependence of the neutron flux is determined via the ^{6}Li(n,α) cross section using a 0.5 mm thick ^{6}Li glass detector at a distance of 430 mm in front of the sample.

Using the gold capture cross section measured at the ORELA facility (Macklin[12]) the Van de Graaff measurements have automatically the same absolute normalization. The samples, metallic (^{176}Hf) or oxide powder (all other cases) pressed to self-supporting tablets, were sealed in ~ 10 μm thin Mylar foil bags. The amounts and compositions of the samples can be found in Table II.

Data reduction according to Eq. (1) first yields an effective capture cross section σ' related to the isotopic cross sections by

$$\sigma' = \sigma_x + \sum_j H_j \sigma_j E_j^* / H_x E_x^* \ , \tag{3}$$

where x stands for the respective isotopic capture cross section to be determined. The calculation of σ_x for ^{160}Dy, ^{170}Yb, ^{176}Lu, and ^{176}Hf, according to Eq. (3), therefore required additional data to correct for the respective isotopic impurities. This necessitated the measurements on ^{171}Yb, ^{161}Dy, ^{175}Lu, and ^{177}Hf. The minor impurities of the other isotopes were taken into account using previous results.[9,13,14]

In the energy range between 2.5 and 10 keV the energy resolution of the ORELA measurements was sufficient to resolve individual resonances. The resonance widths were, in general, found to be narrow compared to the energy resolution. Therefore, only the quantity $g\Gamma_n\Gamma_\gamma/\Gamma$ which is proportional to the resonance area can be extracted. g stands for the statistical spin factor $(2J+1)/[2(2I+1)]$ with compound spin J and target spin I, and Γ_n, Γ_γ, and Γ are the neutron, radiative, and total widths of the resonance. For some resonances Γ is larger than about an eighth of our resolution, so that separate values of $g\Gamma_n$ and Γ_γ can be derived with some confidence. The analysis of the resonances was carried out with the computer code LSFIT (Macklin[15]). In Fig. 1 some of the resonance fits are shown. All the results are listed in Table III.

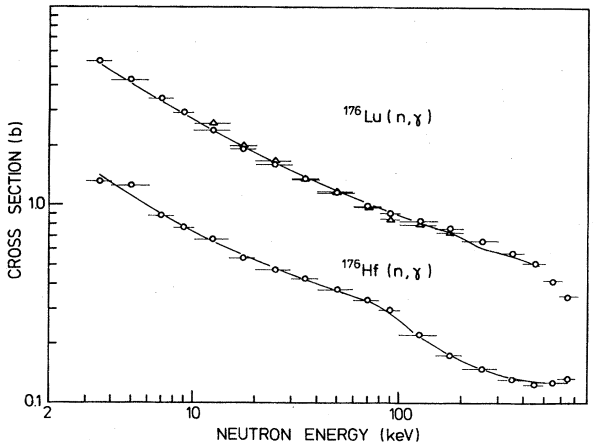

FIG. 2. Effective cross sections for ^{176}Hf(n,γ) and ^{176}Lu(n,γ). Open circles represent the ORELA measurements, open triangles the VDG measurements. The curves are a statistical model fit to the data.

The final effective cross sections of ^{160,161}Dy, ^{175,176}Lu, ^{176,177}Hf, and ^{170,171}Yb averaged over various energy intervals in the whole energy regions of the measurements are listed in Table IV. These data were parametrized in terms of strength functions. The computer code for this analysis (FITACS, Fröhner[16]) adjusts strength functions, radiation widths, and level spacings. These data are summarized in Table V. In Fig. 2 the results for ^{176}Lu and ^{176}Hf are displayed.

Maxwellian averaged capture cross sections $\langle \sigma v \rangle / v_T$ were computed from the differential data for a thermal energy $kT = 30$ keV by numerical integration according to the following formula:

$$\frac{\langle \sigma v \rangle}{v_T} = \frac{2}{\sqrt{\pi}} \int_0^\infty \sigma(E) E \exp(-E/kT) dE \Big/ \int_0^\infty E \exp(-E/kT) dE \ . \tag{4}$$

In practice it is sufficient to carry out the integration between 1 and 200 keV. This cutoff of the integrals leads to an error well within other current uncertainties. The cross section below 2.6 and 5 keV, respectively, was extrapolated. The results of the calculations are shown in Table V.

The various uncertainties of the individual measurements (Table VI) were combined by quadratic error propagation

$$\left[\frac{\Delta\sigma_x}{\sigma_x}\right]^2 = \left[\frac{\sigma'}{\sigma_x} - \frac{H_k E_k^* \sigma_k}{H_x E_x^* \sigma_x}\right]^2 \sum_1 \left[\frac{\Delta\sigma_1'}{\sigma_1'}\right]^2 + \sum_j \left[\frac{H_j E_j^* \sigma_j}{H_x E_x^* \sigma_x}\right]^2 \left[\frac{\Delta\sigma_j}{\sigma_j}\right]^2 . \tag{5}$$

Most of the errors, such as the uncertainty in the multiple scattering correction, are related to the effective cross section σ' represented by the first term of Eq. (5). The index k stands for an isotope measured along with the isotope x; therefore the uncertainties are correlated. The second term in Eq. (5) accounts for the errors in the minor impurities which were taken from literature.

The comparison of the present measurements with previous Van de Graaff results is mainly a problem of the right flux normalization. The activation measurement on ^{176}Lu (Ref. 3) and the Moxon-Rae measurements on ^{170}Yb and ^{175}Lu (Ref. 7) were related to the evaluated nuclear data file B/IV (ENDFB/IV) ^{197}Au capture standard.[18] Table V also shows in brackets cross section values normalized to the ENDFB/IV gold standard for this work.

TABLE III. Resonance parameters of resolved resonances. The stated uncertainties are statistical only. d is probable doublet or multiplet.

Target nucleus	E_0 (eV)	$\frac{g\Gamma_n\Gamma_\gamma}{\Gamma}$ (meV)	E_0 (eV)	$\frac{g\Gamma_n\Gamma_\gamma}{\Gamma}$ (meV)	E_0 (eV)	$\frac{g\Gamma_n\Gamma_\gamma}{\Gamma}$ (meV)
^{160}Dy	2657	19.9±1.9			3398	31.8±3.7
	2664	54.2±2.4			3407	95.8±5.1
	2697	7.3±1.4			3425	43.6±3.9
	2718	20.6±1.8			3438	9.1±2.7
	2744	54.8±2.2			3457	21.7±3.4
	2770	54.9±2.4			3492	45.2±4.0
	2840	17.1±2.0			3504	25.9±3.5
	2850	47.2±2.4			3531	26.7±3.1
	2889	34.2±2.4			3582	54.2±6.0
	2902	53.1±2.5			3586	50.3±4.9
	2910	26.7±2.0			3613	8.8±2.4
	2918	8.5±2.0			3628	31.5±2.7
	2937	61.7±2.7			3672	61.1±3.5
	2991	67.5±2.8			3694	52.1±3.2
	3029	59.5±2.7			3717	56.5±3.2
	3050	48.2±2.3			3728	11.9±3.0
	3084	28.4±3.2			3748	42.1±3.2
	3119	59.6±3.5			3756	29.2±3.2
	3171	54.5±3.5			3797	57.8±3.8
	3231	44.0±3.4			3838	14.4±2.7
	3261	14.6±2.9			3864	53.0±3.4
	3275	101.1±1.7 d			3896	19.6±3.1
	3328	49.4±4.1			3913	70.4±3.7
	3363	43.0±4.1			3936	78.9±3.8
^{176}Hf	2708	4.8±0.9	3633	38.1±1.6	4372	47.0±1.9
	2744	19.6±1.4	3646	36.7±1.7	4386	36.4±1.8
	2781	36.8±1.6	3676	44.4±1.9	4435	42.1±2.0
	2867	31.2±1.4	3704	19.2±1.5	4453	11.3±1.6
	2902	24.3±1.4	3744	4.5±1.2	4480	42.1±2.9
	2945	32.4±1.6	3766	35.5±1.8	4487	42.6±2.3
	2952	34.1±1.7	3788	8.9±1.5	4501	43.1±2.0
	3000	31.5±1.7	3800	9.4±1.3	4543	48.6±1.8
	3021	23.9±1.5	3834	6.7±1.4	4558	51.8±1.8
	3045	36.8±1.6	3860	5.4±1.3	4604	41.0±1.9
	3159	36.6±1.8	3877	8.3±1.5	4614	34.7±1.8
	3207	35.7±1.8	3898	41.5±1.5	4622	10.1±1.9
	3218	40.8±1.8	3927	36.1±1.5	4678	9.6±1.3
	3246	3.2±1.0	3943	3.0±1.2	4698	11.6±1.4
	3253	2.5±0.9	3966	3.0±1.1	4722	7.6±1.5
	3262	15.1±1.1	3987	38.4±1.7	4737	20.1±2.7
	3273	20.5±1.2	4020	21.6±1.4	4743	27.4±2.2
	3293	27.6±1.3	4049	3.8±1.2	4755	36.0±1.8
	3306	7.9±1.1	4067	23.7±1.5	4766	28.4±1.7
	3331	32.4±1.3	4088	5.1±2.3	4831	44.9±2.0
	3343	15.1±1.1	4092	4.6±1.8	4846	11.3±1.6
	3362	5.5±0.9	4118	30.4±1.5	4893	78.7±2.9
	3389	34.4±1.3	4134	44.9±1.7	4911	9.6±1.9
	3397	8.7±1.2	4146	38.6±1.7	4924	31.4±2.3
	3420	42.4±1.5	4159	5.5±1.2	4956	12.3±2.0
	3449	37.9±1.4	4171	33.5±1.5	4984	9.0±2.0
	3465	35.2±1.4	4187	5.6±1.2	5001	33.8±2.4
	3486	10.4±1.1	4204	5.5±1.4	5011	35.8±2.4
	3499	8.0±1.1	4229	40.2±1.9	5020	25.6±2.7
	3524	36.6±1.6	4245	26.6±1.6	5054	45.5±2.5
	3552	3.9±1.2	4265	19.3±1.4	5089	49.4±2.5
	3565	33.4±1.6	4280	39.3±1.8	5108	40.0±2.3
	3599	19.0±1.5	4296	13.2±1.5	5141	39.7±2.4

TABLE III. (*Continued.*)

Target nucleus	E_0 (eV)	$\frac{g\Gamma_n\Gamma_\gamma}{\Gamma}$ (meV)			E_0 (eV)	$\frac{g\Gamma_n\Gamma_\gamma}{\Gamma}$ (meV)
	3616	2.7±1.2	4322	42.6±1.9	5159	52.1±2.7
^{176}Hf	5175	49.4±2.7				
	5199	25.8±2.2				
	5229	35.0±2.6				
^{177}Hf	2653	28.8±1.6				
	2658	11.8±1.4				
	2664	37.1±0.5				
	2671	41.5±0.5				
	2677	10.1±1.4				
	2685	8.0±1.5				
	2696	111.8±0.3 d				
	2707	8.2±1.6				
	2712	22.8±1.7				
	2718	24.8±1.6				
	2726	31.5±1.8				
	2740	133.1±0.4				
	2746	7.1±2.0				
	2755	15.8±1.5				
	2761	26.9±1.7				
	2767	16.0±1.5				

The good agreement between these results and the respective data from literature is especially reassuring as different techniques for the measurements were applied.

B. Solar system abundances

The parameters of interest in the ^{176}Lu cosmic clock evaluation are the ratios of refractory elements Lu/Dy and Lu/Hf, and possibly of other heavy rare earths (HREE's), such as Yb. The principle that the chondritic meteorites and all large inner solar system bodies such as the Earth possess these elements in the solar (and probably the averaged galactic) abundance ratio is well established, and we follow this convention in using data from chondrites to evaluate Lu/Dy and Lu/Hf for the whole solar system and galaxy.

There are, unfortunately, severe limitations on the existing data base for these ratios. Firstly and most generally,

TABLE IV. Histogram of the average neutron capture cross sections of ^{160,161}Dy, ^{175,176}Lu, ^{176,177}Hf, and ^{170,171}Yb.

Energy interval (keV)	σ (mb) ^{160}Dy VDG	^{160}Dy ORELA	^{161}Dy VDG	^{161}Dy ORELA	^{175}Lu VDG	^{176}Lu VDG	^{176}Lu ORELA	^{176}Hf ORELA	^{177}Hf ORELA	^{170}Yb VDG	^{171}Yb VDG
3–4		2331		7651			5360	1313	5056		
4–6		1621		5602			4272	1246	4033		
6–8		1329		4706			3450	880	3104		
8–10		1238		3946			2925	769	2686		
10–15	1276	1027	3430	3313	1892	2452	2378	671	2136	1000	2139
15–20	973	823	2787	2765	1529	1918	1914	537	1763	829	1743
20–30	842	705	2372	2260	1323	1639	1597	473	1445	780	1555
30–40	684	623	2000	1817	1034	1328	1348	425	1193	738	1321
40–60	620	574	1579	1422	899	1154	1147	375	1021	630	1199
60–80	520	492	1229	1144	752	965	985	333	892	557	993
80–100	447	445	993	933	664	850	907	298	798	473	767
100–150	361	335	767	732	583	800	832	223	704	369	593
150–200	303	279	548	545	484	734	764	176	610	298	434
200–300		241		397			663	151	531		
300–400		206		299			575	133	425		
400–500		208		753			512	125	372		
500–600		202		229			420	129	335		
600–700		210		190			351	135	287		

TABLE V. Average resonance parameter from a statistical model fit and Maxwellian averaged capture cross sections $\langle \sigma v \rangle / v_T$ for a thermal energy $kT = 30$ keV. The cross section values in parentheses are calculated relative to Au for ENDFB/IV (Ref. 18) for comparison with the data from previous work.

Target nucleus Az		Strength function $S_l \times 10^4$ $l=0$	$l=1$	$l=2$	$\Gamma_\gamma/D_l \times 10^4$ $l=0$	$l=1$	$\frac{\langle \sigma v \rangle}{v_T}$ (mb) Present work ORELA	VDG	Previous work
^{160}Dy	ORELA	0.37±0.06	0.7 ±0.2	0.15±0.06	155 ± 24	58 ± 9	699±35		
	VDG	0.8 ±0.1	1.1 ±0.4	1.4 ±0.2	86 ± 4	37 ± 2		777±39	
^{161}Dy		1.27±0.05	1.3 ±0.2	1.0 ±0.2	1518 ± 60	333 ± 6	1936±88	2077±75	
^{170}Yb		0.60±0.06	1.29±0.08	0.21±0.08	46 ± 1	110 ± 4		738±29(788)	766±30[b]
^{171}Yb		2.1 ±0.3	2.5 ±0.3	1.8 ±0.5	159 ± 5	204 ± 8		1411±51	
^{175}Lu		0.92±0.04	0.5 ±0.2	2.0 ±0.2	516 ± 19	120 ± 4	1206±54[a]	1179±44(1223)	1266±43[b]
^{176}Lu		1.6 ±0.2	1.7 ±0.4	2.4 ±0.6	318 ± 16	336 ± 22	1526±69	1514±56(1614)	1718±85[c]
^{176}Hf		2.9 ±0.3	0.87±0.07	2.0 ±0.2	12.7±0.2	43.3±0.5	458±20		
^{177}Hf		1.46±0.03	1.0 ±0.05	2.10±0.07	320 ± 2	354 ± 3	1366±61		

[a]Reference 17.
[b]Reference 7.
[c]Reference 3.

TABLE VI. Typical uncertainties in the Van de Graaff (VDG) and ORELA measurements.

	VDG (%)	ORELA (%)
Flux normalization	3	3
Isotopic impurities	0.1–1.6	0.1–1.6
Multiple scattering	1–2	1–2
Gamma attenuation	0.5–1	0.5–1
Pulse height weighting	1–2	1–2
Background subtraction	0.8–1.9	0.3–2
Sensitivity to scattered neutrons	<0.5	<1.6
Electronic drifts and beam intensity fluctuations	0.3–0.6	<0.4
Detector bias	<0.5	0.4
Statistics	0.2–1.7	0.3–1.7
Resonance shape (unknown spin, resolution function)		<3

all abundance table compilations, including the recent ones (Cameron[19] and Anders and Ebihara[20]), must inevitably mix analyses by different techniques. We are taking the standpoint that thermal mass spectrometric isotope dilution (ID) is an inherently superior technique for both accuracy and precision, provided that the sample dissolution is performed in a rigorous way. Secondly, there are no simultaneous analyses of relevant HREE and Hf included in the abundance tables, except for the spark-source data of Knab[21] who did not analyze Lu. The other two data sources for Hf used by Anders and Ebihara,[20] namely the ID study of Shima[22] and the instrumental neutron activation (INAA) data of Ganapathy *et al.*,[23] did not include rare earth (REE) concentrations. The data for REE alone is actually quite good (Nakamura[24] and Evensen *et al.*[25]). However, even though chondrites usually contain refractory elements in constant ratios, they include differing proportions of volatile elements (alkalis, halogens, sulfur, etc.), so that absolute concentrations vary, and combining refractory-element results from different nonsimultaneous determinations can lead to error. A third and related difficulty appears because the only existing simultaneous ID data for Lu/Hf (Patchett and Tatsumoto[26]) show a ratio ~15% higher than current abundance tables (Cameron[19] and Anders and Ebihara[20]). In fact, the Lu/Hf of those tables is clearly lower than any of the simultaneous ID results for six different chondrites from Patchett and Tatsumoto,[26] and this discrepancy needed to be clarified. Fourthly, difficulty with existing abundance data is that Patchett and Tatsumoto[26] did not analyze Dy or any other elements except Lu and Hf, and only obtained data for ordinary chondrite, carbonaceous C2 and C3 material, while C1 was omitted.

To correct all these shortcomings and discrepancies, we undertook at the Max Planck Institut (MPI) a simultaneous thermal ID study of the type C1 carbonaceous chondrite Orgueil for all REE and Hf. We also analyzed simultaneously for K, Rb, Cs, Sr, and Ba to check whether our sample was representative of C1 material for these

more abundant elements.

Our enriched isotopic tracers are in three solutions, one for Lu-Hf, one for all REE, and a third for alkalis and alkaline earths. They were calibrated in quadruplicate against standard solutions containing the normal element, carefully prepared from REE metals, oxides baked to red heat, or NBS standard stoichiometric compounds. Frequently, calibrations were performed against two totally independently prepared standards, and agreement at the 0.1% level was always obtained. Our tracer solutions produce results for the U.S. Geological Survey (USGS) standard rock BCR-1 (Table VII) which agree with means of published data (White and Patchett[28]), and both the REE and Lu-Hf tracer solution give an identical Lu result for BCR-1. The Lu-Hf tracer solution was used to generate a Lu-Hf isochron for meteorites of known age (Patchett and Tatsumoto[27] and Tatsumoto *et al.*[29]) leading to a ^{176}Lu decay constant determination which is confirmed at the 0.5% level by a recent high-quality physical measurement (Sguigna *et al.*[30]). For all these reasons, we believe that our isotopic tracers do not generate any systematic biases. In order to ensure total solution of the Orgueil sample, the dissolution with mixed $HF + HNO_3$ were performed in two steps. Most of the meteorite was reacted in the open dissolution bomb on a hotplate, and after evaporation of those acids, new full-strength acids were added and the bomb sealed and placed in an oven at 180 °C for one week. The analyses were totally spiked with isotopic tracers and to check reproducibility, two 1 g fractions of the same manually ground Orgueil sample were independently processed. Background contamination (blank) levels for the total chemical separation were uniformly low. Ratios of sample element to blank element (Table VII) exceed 800 in all cases except Ba with 260. We therefore made no blank corrections.

The results of the two analyses (Table VIII) agree very closely, and any small difference up to 1% are usually correlated (e.g., Rb with Cs, Ba with Sr, and Hf with Lu) suggesting minor sample heterogeneity as the cause. This agreement vindicates our dissolution procedure and other aspects of the analytical technique. The essential agreement of K, Rb, Cs, Sr, and Ba values with the mean of published values (Table VII) shows that our Orgueil material is representative of Orgueil in general. However, our results do both show 2—3 % underabundance of Ce and 2—3 % overabundance of Yb relative to chondritic means (Nakamura[24] and Evensen *et al.*[25]). This effect has been seen before from ID analyses in Orgueil (Nakamura[24]), and in view of our careful tracer calibrations and concordant results for standard rocks, we must regard it as real. Ce and Yb are the most volatile of the REE, and show for this reason both positive and negative anomalies in refractory white inclusions of carbonaceous chondrites (Grossman and Ganapathy[31]). The most likely explanation for this effect sometimes seen in Orgueil is therefore an under or over abundance of the refractory inclusion component. Thus the Yb abundance is not well fixed from our data.

The new data are compared to published ID data and to abundance table compilations in Table VIII. There is good agreement for Lu/Dy between all sources, and the mean of our two Lu/Dy ratios is exactly the same as the Anders and Ebihara[20] value. None of the published high-quality ID data for REE included Hf, however, and our new simultaneous results disagree with the abundance tables for REE/Hf ratios. Apart from all the analytical reasons mentioned above, we have confidence in our REE/Hf ratios because the Orgueil Lu/Hf ratio results agree well with Lu/Hf determined on C2 Murchison and the C3 Allende standard powder in Denver using the same tracer solution (Patchett and Tatsumoto[26]). The C2 Murchison result was used to define a Hf isotopic growth curve for undifferentiated solar system material (Patchett *et al.*[32]), and the close agreement of the new Orgueil re-

TABLE VII. Abundances in C1 meteorite Orgueil.

Element	Sample/blank[a] ($\times 10^3$)	BCR-1[b] (ppm)	Orgueil-1 (ppm)	Orgueil-2 (ppm)	Literature[c] (ppm)
K	44	14 187.0	542.5	548.6	569
Rb	105	46.78	2.34	2.29	2.30
Cs	94	0.956	0.189	0.187	0.186
Sr	33	332.20	7.25	7.26	7.91
Ba	0.26	675.80	2.40	2.42	2.27
La	0.82	24.94	0.238	0.235	0.236
Ce	2.2	53.40	0.613	0.611	0.619
Nd	4.7	28.83	0.467	0.467	0.462
Sm	3.8	6.59	0.153	0.153	0.142
Eu	5.8	1.96	0.0579	0.0581	0.0543
Gd		6.64	0.206	0.205	0.196
Dy	12.7	6.42	0.254	0.254	0.242
Er	8.3	3.67	0.166	0.165	0.160
Yb	11.3	3.37	0.170	0.170	0.166
Lu	2.5	0.497	0.0253	0.0254	0.0243
Hf	0.85	4.97	0.1061	0.1071	0.119

[a]Ratio of element from 1 g Orgueil to background contamination for the whole analytical procedure.
[b]U.S. Geological Survey standard basalt rock powder.
[c]Values from Anders and Ebihara (Ref. 20).

TABLE VIII. Abundance ratios for ^{176}Lu clock evaluation.

		Lu/Dy atomic	Lu/Hf atomic
Cameron[a]	Abundance table	0.0946	0.206
Anders and Ebihara[b]	Abundance table	0.0927	0.210
Nakamura[c]	C1 Orgueil	0.0934	
	C2 Murchison	0.0942	
	10 chondrites	0.0918	
Evensen *et al.*[d]	C1 mean	0.0928	
Patchett and Tatsumoto[e]	C2 Murchison		0.241
	C3 Allende		0.236
This study	C1 Orgueil	0.0925	0.243
	C1 Orgueil	0.0929	0.242
Best values used here		0.0927	0.243

[a]Reference 19.
[b]Reference 20.
[c]Reference 24.
[d]Reference 25.
[e]Reference 26.

sults confirms this growth curve as the correct one, which is therefore now based on fully concordant C1, C2, and C3 Lu/Hf ratios. The Lu/Hf ratios given in the two recent abundance tables are ~13% lower (Table VIII), and would lead to a present-day Hf isotopic composition completely inconsistent with Hf isotopic variation patterns on the Earth. If the Lu/Hf values of Anders and Ebihara[20] or Cameron[19] were the correct chondritic one, then the terrestrial Lu/Hf ratio would be nonchondritic by ~15%, which would be unlikely for two highly refractory elements in a major solar system body. Our C1-C2-C3 Lu/Hf ratio leads to self-consistency for the Earth, and this is additional evidence that our Lu/Hf ratio is the correct chondritic one.

In view of the low quality and dispersion of chondritic Hf data, Anders and Ebihara[20] accepted only three data sources. The first of these, the INAA study by Ganapathy *et al.*[23] agrees closely with results from our Hf tracer for Orgueil, Murchison, and Allende and needs no further discussion. The Hf ID concentrations of Shima[22] were corrected downwards by up to 12% for an average background contamination, in spite of which results for Orgueil, Murchison, Allende, and Richardton were systematically 10% or more higher than those of Patchett and Tatsumoto[26] and this study. We take the view that such large blank corrections are unacceptable for determination of critical solar system abundances, and note that our sample/blank ratios of >800 for HREE and Hf mean that no corrections to our data were necessary. The spark-source mass spectrometric data of Knab[21] show Hf levels more comparable to ours for Murchison and Allende, but agree with Shima[22] for Orgueil, and this had a large influence on the abundance table of Anders and Ebihara,[20] leading to deemphasis of the Chicago INAA data, which agree with ours. We note that although Knab[21] did not analyze Lu, his Dy/Hf ratios for Orgueil, Murchison, and Allende vary by up to 30%, while the presumably equivalent Lu/Hf ratio varies by only 3% in the ID data from our Lu-Hf tracer (Table VIII). This clearly suggests a much lower precision and accuracy in his technique than in ours.

We conclude that our simultaneous ID data are clearly superior for Dy/Lu/Hf ratios to all published results, and that the optimum values for ^{176}Lu clock evaluation are as given at the bottom of Table VIII. The change we propose to the tables is in Hf, for which a 10% lower abundance of 0.158 atoms/10^6 Si seems appropriate.

III. DISCUSSION

A. *s*-process nucleosynthesis

Before we start to analyze the ^{176}Lu cosmic clock we need a description of the heavy elements around ^{176}Lu. This is required firstly because we have to recalculate the original ^{176}Lu abundance from ^{160}Dy selected as a suitable stable *s*-only nucleus below ^{176}Lu, and secondly, to determine *s*-process neutron density and temperature which are important if the ^{176}Lu half-life turns out to be temperature sensitive.[7]

It was Seeger *et al.*[33] who first showed that an exponential distribution of neutron exposures produces a reasonable fit to the observed heavy element abundances. They already showed that a simple model of galactic nuclear evolution can account for the exponential distribution. This astrophysically meaningful model was in the following years refined by the inclusion of a "weak" component of exposure distributions to reproduce the abundances below $A=90$ (Refs. 34 and 35), and further substantiated by stellar *s*-process models[36,37] where the exponential fluence distribution is a natural consequence of the repeated occurrence of a pulsed *s* process.

In this investigation we follow the concept of an exponential fluence distribution as used in this previous work. Additionally, branchings of the *s*-process path were treated according to the theory of Ward *et al.*[4] assuming a steady *s*-process flow. But as it was pointed out by Ulrich[38] this analysis is also valid in the frame of the

pulsed s-process model if the capture cross sections of the branching, as in all presently treated cases, are larger than 500 mb. This guarantees that during the pulse a steady flow is quickly established.

An important prerequisite for an improvement of previous calculations was a new compilation of solar abundances from Anders and Ebihara[20] and an updated set of neutron capture cross sections mainly from the Karlsruhe pulsed 3 MV Van de Graaff accelerator and the Oak Ridge Linear Accelerator ORELA (most references of ORELA data are found in Macklin and Winters[39] and Allen, Boldman, and Macklin[40]).

Figure 3 shows the results of our calculations. In Fig. 3 (top part) the characteristic quantity, Maxwellian averaged capture cross section times s-process abundance, σN, is displayed as a function of mass number from $A=56$ to 209 (σ represents now and for the following discussions always the Maxwellian averaged capture cross section). The indicated data points are s-only nuclei or nuclei produced predominantly by the s process. The solid curve yields the average time integrated neutron flux

$$\tau_0 = 0.30[kT(\text{keV})/30]^{1/2}\ \text{mb}^{-1}$$

by means of a least squares fit to a selected number of s-only isotopes which have well-known solar abundances and are not located in a branching. This last requirement is certainly not strictly correct for some of the chosen isotopes; for instance ^{134}Ba and ^{148}Sm could be affected by neutron capture of their radioactive progenitors ^{134}Cs and ^{148}Pm. Such isotopes were classified as "unbranched" nuclei if the experimental σN value with its quoted uncertainty gave no indication of a branching. The curve is normalized to σN (^{160}Dy), the value of which has been measured in this work. Although ^{160}Dy has a radioactive progenitor, ^{160}Tb, with a terrestrial half-life of 72 d, no branching of the s-process flow can develop because this half-life is reduced under s-process conditions to a few hours.[41–43] This reduction of the half-life is caused by allowed beta decay from excited ^{160}Tb states.

In Fig. 3, (bottom part) the r-process residuals are shown. These abundances are simply generated by a subtraction of the calculated s-process abundances from the solar abundances. As expected, they form a relatively smooth distribution with distinct maxima at $A=129$ and 191. Pure r-process residuals are indicated in full black, squares and circles distinguish between odd and even mass numbers, respectively.

As the pure s-process isotopes are normally shielded only against contributions of the r process we cannot use simply solar abundances, a p-process correction has to be taken into account, although this correction amounts only to a few percent. Unfortunately, the p process is poorly understood and the model calculations[44–46] are too uncertain to determine the p-process components of s-only isotopes. Therefore this p-process contribution was approximated using the abundance of the nearby p-only isotopes. This treatment was checked by comparing the abundances of other neighboring p-only isotopes (^{124,126}Xe, ^{130,132}Ba, and ^{106,108}Cd) and should be a good approximation at least for nuclei far from magic neutron shells. No p correction was applied to odd mass s-only isotopes. Arguments for

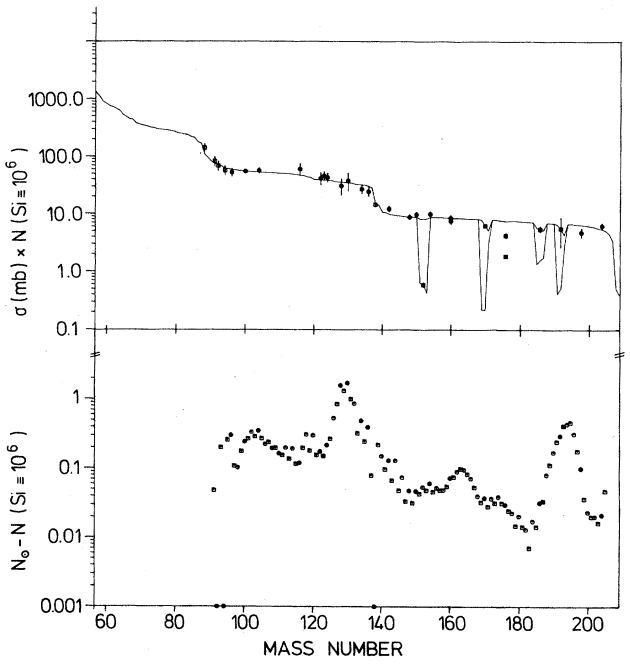

FIG. 3. (Top) the product of s-process abundance times cross section as a function of mass number for $kT=23$ keV. The symbols correspond to empirical values for s-only isotopes or to s-process dominated isotopes near magic neutron shells. Values represented by full black circles are used for a least squares fit to obtain the average time integrated neutron flux τ_0. The curve is normalized to the σN value of ^{160}Dy with the cross section from the VDG measurement. The ORELA value is indicated as an open circle. The error bars of the empirical σN values include uncertainties from the cross sections and the abundances. Significant branchings of the s-process path were identified due to the low empirical σN values of ^{152}Gd, ^{170}Yb, and ^{186}Os. A branching to reproduce the σN values of ^{192}Pt is only tentative. (bottom) Approximate r-process abundances between $A=96$ and 205 were derived as the difference between solar abundances (chiefly from Ref. 20 and the calculated s-process abundances). Even isotopes are given by circles, odd isotopes by squares. Chiefly or pure r-process nuclei are indicated by full symbols.

this decision can be found elsewhere.[47,48]

Significant branchings of the s process close to ^{176}Lu at ^{151}Sm-^{152}Eu, ^{169}Er-^{170}Tm, ^{185}W-^{186}Re, and ^{191}Os-^{192}Ir were considered. Evidences for these branchings are the $\sigma N_\odot$ values of ^{152}Gd, ^{170}Yb, ^{186}Os, and ^{192}Pt falling below the calculated σN curve (Fig. 3). The treatment of the ^{191}Os-^{192}Ir branching was only tentative because $\sigma N_\odot(^{192}\text{Pt})$ is not accurately known. As the mathematical formalism to reproduce $\sigma N_\odot$ of ^{152}Gd and ^{170}Yb has already been reported elsewhere,[7,49] it is sufficient to specify the corresponding equations for the ^{185}W-^{186}Re branching. $\sigma N_\odot(^{186}\text{Os})$ is related to the unbranched σN curve at $A=184$ by the expression

$$\frac{\sigma N_\odot(^{186}\mathrm{Os})}{\sigma N(A=184)} = \frac{\lambda_\beta(^{185}\mathrm{W})}{\lambda_n(^{185}\mathrm{W})}\zeta'(^{186}\mathrm{Re})\zeta'(^{185}\mathrm{W})\zeta(^{185}\mathrm{Re}) \times \left[\frac{\lambda_\beta(^{186}\mathrm{Re})}{\lambda_n(^{186}\mathrm{Re})}\zeta(^{186}\mathrm{Os}) + \frac{\sigma(^{186}\mathrm{Os})}{\sigma(^{186}\mathrm{Re})}\right],$$

with

$$\zeta(^A Z) = \left[1 + \frac{1}{\tau_0 \sigma(^A Z)}\right]^{-1} \quad (6)$$

and

$$\zeta'(^A Z) = \left[\frac{\lambda_\beta(^A Z) + \lambda_{EC}(^A Z) + \lambda_n(^A Z)}{\lambda_n(^A Z)} + \frac{1}{\tau_0 \sigma(^A Z)}\right]^{-1},$$

where λ_β, λ_{EC}, and λ_n are the beta decay, electron capture, and neutron capture rates, respectively. λ_{EC} is relevant only for ^{186}Re. The neutron capture rate is dependent on the neutron density n_n via $\lambda_n(^A Z) = n_n v_T \sigma(^A Z)$, where v_T designates the thermal velocity.

The branchings at ^{169}Er-^{170}Tm and ^{185}W-^{186}Re are chiefly caused by a competition of the s-process capture time with the only weakly temperature sensitive beta half-lives. The ^{151}Sm-^{152}Eu branching is dependent both on the temperature and on the neutron density. The calculations take into account the various uncertainties in the abundances and cross sections, especially of radioactive branch point nuclei. The strong temperature dependence of beta decay half-lives in the ^{151}Sm-^{152}Eu branching was taken from the work of Beer *et al.*[49] In Fig. 4 the result of this analysis is shown. The treated branchings yield values for the neutron density n_n and temperature kT confined to the inner region of the solid curve. A further limitation of allowed pairs of values is obtained using a recent result on the s-process neutron density[50] illustrated by the dashed lines. All parameters obtained in our s-process analysis are summarized in Table IX.

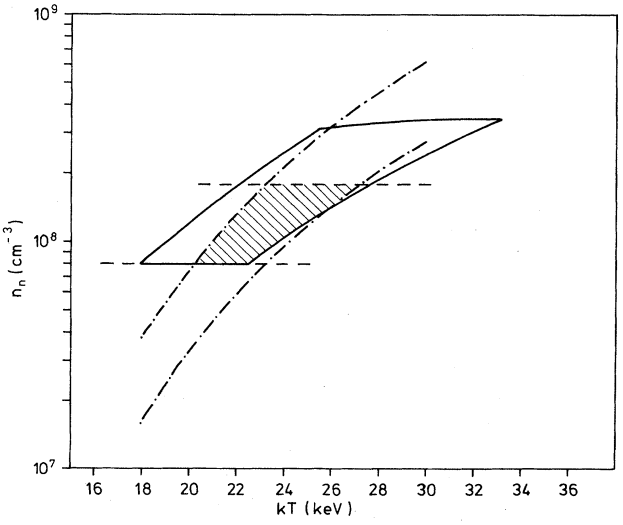

FIG. 4. The s-process neutron density n_n and temperature kT derived from the various branchings. The solid curve shows the allowed range of values calculated from the ^{151}Sm-^{152}Eu, ^{169}Er-^{170}Tm, and ^{185}W-^{186}Re branchings. The dashed lines indicate the limits of the neutron density reported in Ref. 50. The dashed dotted lines designate the range of temperatures and neutron densities from ^{176}Lu treated as a stellar thermometer. The neutron densities and temperatures common to all investigated branchings lie in the hatched region.

TABLE IX. Characteristic quantities of the s-process analysis.

Time integral of the neutron flux τ_0	$(0.30\pm0.01)\left[\frac{kT(\mathrm{keV})}{30}\right]^{1/2}$ mb^{-1}
Average number of captured neutrons per iron seed	12
Fraction of iron seed	0.050%
Duration of s process	200—500 yr
Temperature kT	18—28 keV
Neutron density	$(0.8\text{—}1.8)\times10^8$ cm^{-3}

B. Nucleosynthesis at ^{176}Lu

The isotope ^{176}Lu and stable isotopes in its vicinity are shown in Fig. 5. We can already classify s-, r-, and p-process isotopes simply by the size of their indicated solar abundances. Both ^{176}Lu and ^{176}Hf should belong to the s-process isotopes. This suggests that in spite of the long half-life of ^{176}Lu a branching of the s-process path occurs at that point. This branching can be mediated by an isomeric state at 127 keV with a 3.68 h beta decay half-life.[1–3] Therefore, if ^{176}Lu ($T_{1/2}=3.6\times10^{10}$ yr) is used as a cosmic clock to measure the age of the s process via $R = N(^{176}\mathrm{Lu})/N_\odot(^{176}\mathrm{Lu})$, this branching must be taken into account. The quantity R, the ratio of original and solar system abundance N, and $N_\odot$ can be calculated in two different ways depending on the stable s-only isotope of reference:

$$R = \left[\frac{1}{f_n} + \frac{1}{\tau_0 \sigma(^{176}\mathrm{Lu})}\right]^{-1} \frac{\sigma N_\odot(^{160}\mathrm{Dy})}{\sigma N_\odot(^{176}\mathrm{Lu})} F\delta \quad (7)$$

and

$$R = \delta \frac{1 + \frac{N_\odot(^{176}\mathrm{Hf})}{N_\odot(^{176}\mathrm{Lu})}}{1 + \frac{\sigma(^{176}\mathrm{Lu})}{\sigma(^{176}\mathrm{Hf})}\zeta(^{176}\mathrm{Hf})\left[\frac{1-f_n}{f_n}\right]}. \quad (8)$$

In Eq. (7) ^{160}Dy is the reference isotope whereas in Eq. (8) ^{176}Hf is used. The quantity F is chiefly a product of propagators $\zeta(i)$ from $i=161$ to 175. The factor δ accounts for possible depletion effects of the ^{176}Lu abundance during freeze out at the termination of the s process.

In order to calculate R via Eq. (7) or (8) the branching factor f_n has to be known. If it can be assumed that f_n is determined solely by the population P of the 3.68 h isomeric state via neutron capture on ^{175}Lu,[3] which additionally implies $\delta=1$, we obtain the supplementary equation

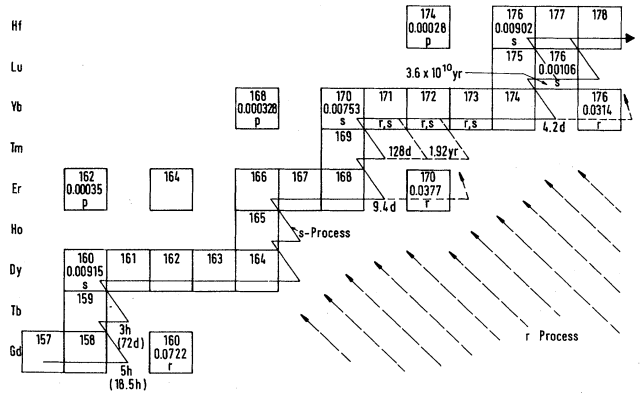

FIG. 5. Various processes that contribute to the mass region around ^{176}Lu. The *s*-process path is shown by the solid line. Competition between neutron capture and beta decay occurs at ^{170,171}Tm and at ^{176}Lu. The branching at ^{176}Lu is mediated by an isomeric state with a beta decay half-life of 3.68 h. Possible *r*-process contributions are indicated by inclined dashed arrows. The terestrial half-life of ^{160}Tb in brackets is reduced to a few hours due to allowed beta decay from excited states so that no branching at ^{160}Tb occurs and ^{160}Dy is a good normalization point for the ^{176}Lu analysis. The indicated abundances are from Ref. 20.

$$f_n^{\text{capt}} = 1 - P = 1 - \sigma^m(^{175}\text{Lu})/\sigma(^{175}\text{Lu}) , \tag{9}$$

where σ^m is the capture cross section to the ^{176}Lu isomer and σ is the total capture cross section. But f_n^{capt} is not necessarily equal to the effective branching factor f_n of Eqs. (7) and (8). Thermal effects at the site of the *s* process can change the initial population. A combination of Eqs. (7) and (8), however, leads to

$$R = \delta \frac{\dfrac{\sigma(^{160}\text{Dy})}{\sigma(^{176}\text{Hf})}\dfrac{N_\odot(^{160}\text{Dy})}{N_\odot(^{176}\text{Lu})}\zeta(^{176}\text{Hf})F - \left[\dfrac{N_\odot(^{176}\text{Hf})}{N_\odot(^{176}\text{Lu})}+1\right]}{\dfrac{\sigma(^{176}\text{Lu})}{\sigma(^{176}\text{Hf})}\dfrac{\zeta(^{176}\text{Hf})}{\zeta(^{176}\text{Lu})}-1} \tag{10}$$

and

$$f_n = \frac{RA - \sigma(^{176}\text{Lu})/\sigma(^{176}\text{Hf})}{\zeta^{-1}(^{176}\text{Hf}) - \dfrac{\sigma(^{176}\text{Lu})}{\sigma(^{176}\text{Hf})} - \dfrac{RA}{\tau_0\sigma(^{176}\text{Lu})}} \tag{11a}$$

with

$$RA = \frac{1 + N_\odot(^{176}\text{Hf})/N_\odot(^{176}\text{Lu})}{\dfrac{\sigma N_\odot(^{160}Dy)}{\sigma N_\odot(^{176}\text{Lu})}\zeta(^{176}\text{Hf})f} . \tag{11b}$$

It is important to note that f_n in Eq. (11) is *independent* from δ, i.e., from any depletion effects of the ^{176}Lu abundance. A comparison of f_n from Eq. (11) with f_n^{capt} from Eq. (9) leads to important conclusions about the reliability of the mean age calculated via Eqs. (10), (7), or (8):

(1) If f_n is equal to f_n^{capt} then *no thermal effects* were present during the ^{176}Lu synthesis ($\delta = 1$), ^{176}Lu is an excellent cosmic clock, and the age can be determined via Eq. (7) or (8) in conjunction with (9) or via Eq. (10).

(2) If f_n and f_n^{capt} are different then *thermal effects were important* in the population of the ^{176}Lu ground and isomeric state. The application of ^{176}Lu as a cosmic clock using Eq. (10) depends now on the freeze out conditions of the ^{176}Lu abundance after termination of the *s* process.

(3) Thermal equilibrium between ground and isomeric state leads to a simple relation between f_n and the stellar temperature kT,

$$f_n = \left[1 + \frac{t_n}{t_\beta}\frac{(2J_m+1)\exp(-E_m/kT)}{\sum_i (2J_i+1)\exp(-E_i/kT)}\right]^{-1} , \tag{12}$$

where J_i and E_i are the spin and excitation energy of state i of ^{176}Lu; J_m and E_m are the spin and excitation energy of the isomer; and t_n, and t_β are the neutron capture and isomeric beta half-lives.

Before we can start to compute R and f_n according to Eqs. (10) and (11) we have to correct for the following effects:

In our treatment of ^{176}Lu so far we have relied on the *s*-only nature of ^{160}Dy, ^{176}Lu, and ^{176}Hf. It is certainly not true that these nuclei are shielded from the *p* process. This is a small contribution but nevertheless important. The *p* contribution to ^{176}Hf and ^{160}Dy were approximated by the nearly *p*-only isotopes ^{174}Hf and ^{156}Dy, respectively. For ^{176}Lu as an odd-odd isotope the *p* process can produce only a negligible abundance.[47,48]

^{175}Yb, the radioactive progenitor of ^{175}Lu, has a laboratory half-life of 4 d which remains unchanged under stellar *s*-process conditions. Therefore, ^{176}Lu and ^{176}Hf are bypassed partially by a small branching to ^{176}Yb. For our neutron density of $(0.8-1.8)\times 10^8$ cm^3, this branching which has been taken into account amounts to (1—2.2) %.

^{160}Dy and ^{176}Hf have 2^+ excited states at $\sim$88 keV which are in the *s*-process environment at $kT = 18-28$ keV occupied by $\sim$(3.5—18) %. ^{176}Lu on the other hand has no such state. A statistical model calculation reported by Harris[51] shows that the cross sections of the 2^+ states are larger by a factor 1.49 than those of the 0^+ states. Therefore, the experimental capture cross sections of ^{176}Hf and ^{160}Dy have to be raised by $\sim$(1.7—9) %.

^{176}Lu has a sizable thermal cross section of 2107 b whereas ^{160}Dy has only 61 b and ^{176}Hf has only 36 b. Therefore, ^{176}Lu could be depleted selectively in meteorites by spallation neutrons from cosmic ray particles. For ^{149}Sm with a thermal cross section of 41 000 b this effect was estimated to be $\leq$4% by Macklin *et al.*[52] Because of the general uncertainty about such depletion effects no correction was applied.

^{176}Yb has an isomeric state with 11.7 s at 1.051 MeV which due to its spin and parity, 8^-, can make an allowed beta transition to the 7^- ^{176}Lu ground state. This situation allows the production of *r* process ^{176}Lu via the population of the ^{176}Yb isomer from the ^{176}Tm decay followed by the fractional ^{176}Yb^m beta decay to ^{176}Lu. The *r*-process contribution can be estimated by

$$\frac{N_r(^{176}\mathrm{Lu})}{N_\odot(^{176}\mathrm{Lu})}=\frac{N_\odot(^{176}\mathrm{Yb})Pf_\beta}{N_\odot(^{176}\mathrm{Lu})} . \quad (13)$$

The isomeric population P according to the Table of Isotopes (Lederer and Shirley[53]) is 0.86% and f_β is estimated to be 0.14%. We obtain with these numbers an r-process correction for ^{176}Lu of only 0.02%.

Using Eqs. (11a) and (11b) the effective branching factor f_n can be calculated. It is clear that this calculation will be strongly influenced by the adopted ^{160}Dy capture cross section as we have a relatively large systematic deviation between the ORELA and Van de Graaff (VDG) values. A usual practice in such a case would be to calculate the average of the two ^{160}Dy cross sections and then derive the effective branching factor f_n. However, as the real size of f_n is of decisive importance, a more conservative attitude is assumed. f_n is calculated independently for both ^{160}Dy values taking into account their respective uncertainties. A lower bound of the branching factor is set by the lower error limit of f_n from the ORELA data and an upper bound is set by the upper limit of f_n from the VDG data. In this way, we ultimately estimated for the effective branching factor $0.39 \leq f_n \leq 0.60$. The limits in f_n also include the uncertainties of the experimental results and a slight variation due to the temperature variation of the cross sections.

Our result of f_n is much higher than the branching factor f_n^{capt} determined from the population of the ^{176}Lu isomer via neutron capture of ^{175}Lu. Allen *et al.*[54] reported a value $f_n^{capt}=0.22\pm0.10$, Beer and Käppeler[3] reported a value of 0.36 ± 0.04. This result must be revised, slightly. With the present total capture cross section of ^{175}Lu we obtain 0.34 ± 0.04. Therefore f_n appears to be different from f_n^{capt}, and consequently the ^{176}Lu isomer is temperature sensitive. This result would be in agreement with the calculations of Beer *et al.*[7] that ^{176}Lu^m is thermally unaffected only below $kT=16$ keV, a value below the temperature limit of the s process ($kT \geq 18$ keV) deduced from the investigated branchings. Nevertheless, by using Eq. (10) our experimental results can be expressed in an s-process age provided the depletion factor δ is known from a detailed stellar s-process model. Presently, we can calculate the ^{176}Lu age only under the extreme assumption $\delta=1$ which actually means no ^{176}Lu depletion. For reasons of comparison with the r-process cosmic clocks we will calculate the ^{176}Lu age $\Delta+4.6$ Gyr in the frame of the exponential model of cosmochronometers (Clayton[55]):

$$R=\frac{\lambda_R-\lambda}{\lambda_R}\frac{1-\exp(-\lambda_R\Delta)}{\exp(-\lambda\Delta)-\exp(-\lambda_R\Delta)} , \quad (14)$$

where λ_R is the rate of nucleosynthesis. According to Fowler[56] it is assumed additionally that this rate at the time of solar system formation is about 9% of the initial rate ($\lambda_R\Delta=1/0.43$). The calculated ^{176}Lu age $\Delta+4.6$ Gyr is temperature dependent. For $kT=18$, 23, and 28 keV it is $\gtrsim$25.6, 32.1, and 37.1 Gyr, respectively, taking into account the various uncertainties. This limit of the ^{176}Lu age is higher than the highest r-process age of 21^{+2}_{-4} Gyr determined via the U/Th clock.[57] This high r-process age has been recently revised, however, to (17.6 ± 4) Gyr.[58]

As discussed by Beer *et al.*[7] and Beer[8] an additional application of ^{176}Lu is as a thermometer of the s process. This presumes that the ground and isomeric states of ^{176}Lu are in thermal equilibrium. Beer *et al.*[7] have derived lower temperature bounds for this equilibrium process which are dependent on the degree of K forbiddenness of certain interband transitions. Apart from extreme assumptions for this K forbiddenness our limit on the s-process temperature ($kT \geq 18$ keV) is identical with the temperature limit which characterizes ^{176}Lu as a stellar thermometer.[7] Using Eq. (12) we have calculated temperature and neutron density under the assumption of thermal equilibrium of the ^{176}Lu ground and isomeric states. Figure 5 shows the result of this calculation between $kT=18$ and 30 keV. This new range of temperature and neutron density values yields further constraints for the allowed region of s-process temperatures which lies now between $kT=20$ and 27 keV.

IV. CONCLUSIONS

In the present investigation we have determined neutron capture cross sections and solar abundances of the isotopes ^{160,161}Dy, ^{170,171}Yb, ^{175,176}Lu, and ^{176,177}Hf. These data have important astrophysical impact for the s-process nucleosynthesis in general and especially for the nucleosynthesis of ^{176}Lu.

The s-process synthesis path was calculated from $A=90$ to 209 including the analysis of significant s-process branchings. The average time integrated neutron flux was determined to be

$$0.30\left[\frac{kT(\mathrm{keV})}{30}\right]^{1/2}\mathrm{mb}^{-1}$$

and the s-process neutron density and temperature were found to be $n_n=(0.8-1.8)\times10^8$ cm^{-3}, $kT=18$–28 keV, respectively.

The ^{176}Lu clock was analyzed using the current model for cosmochronometers.[55] The high ages found compared to the r-process ages suggests that the ^{176}Lu abundance was subject to a depletion probably during freeze out at the termination of the s process. This interpretation is in agreement with the probable temperature sensitivity of the ^{176}Lu isomeric state. This temperature dependence induced by internal electromagnetic transitions may even cause thermal equilibrium between the ground and isomeric states. The calculated temperature and neutron densities under this assumption are in good agreement with the respective values derived from branchings.

The present results can certainly be greatly improved by more accurate data. This is true, for example, for the capture cross sections of the radioactive branch point nuclei where we had to rely on theoretical estimates. More accurate capture cross sections and solar abundances of s-only isotopes are also desirable.

The procedure used here of measuring the same cross section with two totally different experimental configurations proved to be very helpful in detecting hidden systematic uncertainties. Finally it should be pointed out that the precision of the important σN values acting as normalization points seems to be actually limited to a few

percent because p-process corrections and excited state capture introduce uncertainties which are presently hard to overcome.

ACKNOWLEDGMENTS

We are grateful to M. Tatsumoto for passing on to us the sample of Orgueil originating from P. Pellas, Museum d'Histoire Naturelle, Paris. W. M. White cooperated in the preparation of standards at MPI Mainz, and provided most of the results for BCR-1. We thank E. Anders for his comments on the solar Hf abundance. We appreciate the efforts of A. Ernst, H. Gündert. E.-P. Knaetsch, and D. Roller of the Van de Graaff operation staff to keep the machine in an excellent condition during the experiment. One of the authors (H.B.) is indebted to Richard Ward for pointing out an error in Eq. (2) of Ref. 8. This has the consequence that Eq. (10) is a mathematically exact solution, not (as it was derived in Ref. 8) an approximation good only for $1/\tau_0\sigma(^{176}\mathrm{Lu}) \ll 1$. Numerically this difference is negligibly small.

[1]J. Audouze, W. A. Fowler, and D. N. Schramm, Nature (London) **238**, 8 (1972).
[2]M. Arnould, Astron. Astrophys. **22**, 311 (1973).
[3]H. Beer and F. Käppeler, Phys. Rev. C **21**, 534 (1980).
[4]R. A. Ward, M. J. Newman, and D. D. Clayton, Astrophys. J. Suppl. **31**, 33 (1976).
[5]R. A. Ward, Astrophys. J. **216**, 540 (1977).
[6]H. Beer and F. Käppeler, in *Proceedings of the Fourth International Conference on Neutron Capture Gamma-Ray Spectroscopy and Related Topics, Grenoble,* IOP Conf. Series No. 62 (Institute of Physics and Physical Society, London, 1981), p. 558.
[7]H. Beer, F. Käppeler, K. Wisshak, and R. A. Ward, Astrophys. J. Suppl. **46**, 295 (1981).
[8]H. Beer, Astrophys. J. **262**, 739 (1982).
[9]H. Beer and R. L. Macklin, Phys. Rev. C **26**, 1404 (1982).
[10]J. Almeida and F. Käppeler, Astrophys. J. **265**, 417 (1983).
[11]R. L. Macklin, J. Halperin, and R. R. Winters, Nucl. Instrum. Methods **164**, 213 (1979).
[12]R. L. Macklin (unpublished).
[13]V. S. Shorin, V. N. Kononov, and E. D. Poletaev, Yad. Fiz. **19**, 5 (1974) [Sov. J. Nucl. Phys. **19**, 2 (1974)].
[14]V. N. Kononov, E. D. Poletaev, B. D. Yurlov, M. V. Bokhavko, L. E. Kazakov, and V. M. Timokhov, in *Proceedings of the Fourth International Conference on Neutron Capture Gamma-Ray Spectroscopy and Related Topics, Grenoble,* IOP Conf. Series No. 62 (Institute of Physics and Physical Society, London, 1981), p. 518.
[15]R. L. Macklin, Nucl. Instrum. Methods **59**, 12 (1976).
[16]F. Fröhner, private communication (see also F. Fröhner, B. Goel, and V. Fischer, in Proceedings of the NEANDC/NEACRP Specialist's Meeting on Fast Neutron Capture Cross Sections, Argonne, 1982, edited by A. B. Smith and W. P. Poenitz, Argonne National Laboratory Report ANL-83-4, 1983, p. 116.
[17]R. L. Macklin, D. M. Drake, and J. J. Malanify, Los Alamos National Laboratory Report LA-7479-MS, 1978 (unpublished).
[18]Brookhaven National Laboratory Report ENDFB/IV BNL-17451 (ENDF-201), 1975, edited by D. Garber.
[19]A. G. W. Cameron, in *Essays in Nuclear Astrophysics,* edited by C. A. Barnes, D. N. Schramm, and D. D. Clayton (Cambridge University, Cambridge, 1983), p. 23.
[20]E. Anders and M. Ebihara, Geochim. Cosmochim. Acta **46**, 2363 (1982).
[21]H. J. Knab, Geochim. Cosmochim. Acta **45**, 1563 (1981).
[22]M. Shima, Geochim. Cosmochim. Acta **43**, 353 (1979).
[23]R. Ganapathy, G. M. Papia, and L. Grossman, Earth Plane. Sci. Lett. **29**, 302 (1976).
[24]N. Nakamura, Geochim. Cosmochim. Acta **38**, 757 (1974).
[25]N. M. Evensen, P. J. Hamilton, and R. K. O'Nions, Geochim. Cosmochim. Acta **42**, 1199 (1978).
[26]P. J. Patchett and M. Tatsumoto, *Abstracts Lunar and Planetary Science Conf. XII* (Lunar and Planetary Institute, Houston, 1981), p. 822.
[27]P. J. Patchett and M. Tatsumoto, Nature (London) **288**, 571 (1980).
[28]W. M. White, P. J. Patchett, Earth Plane. Sci. Lett. **67**, 167 (1984).
[29]M. Tatsumoto, D. M. Unruh, and P. J. Patchett, Proceedings of the 6th Symposium on Antarctic Meteorites, Tokyo, 1981, p. 237.
[30]A. P. Sguigna, A. J. Larabee, and J. C. Waddington, Can. J. Phys. **60**, 361 (1982).
[31]L. Grossman and R. Ganapathy, Geochim. Cosmochim. Acta **40**, 331 (1976).
[32]P. J. Patchett, O. Kouvo, C. E. Hedge, and M. Tatsumoto, Contrib. Mineral. Petrol. **78**, 279 (1981).
[33]P. A. Seeger, W. A. Fowler, and D. D. Clayton, Astrophys. J. Suppl. **11**, 121 (1965).
[34]R. A. Ward and M. J. Newman, Astrophys. J. **219**, 195 (1978).
[35]F. Käppeler, H. Beer, K. Wisshak, D. D. Clayton, R. L. Macklin, and R. A. Ward, Astrophys. J. **257**, 821 (1982).
[36]R. K. Ulrich, in *Explosive Nucleosynthesis,* edited by D. N. Schramm and W. D. Arnett (University of Texas, Austin, 1973), p. 139.
[37]J. W. Truran, and I. Iben, Jr., Astrophys. J. **216**, 197 (1977).
[38]R. K. Ulrich, in *Essays in Nuclear Astrophysics,* edited by C. A. Barnes, D. N. Schramm, and D. D. Clayton (Cambridge University, Cambridge, 1983), p. 301.
[39]R. L. Macklin and R. R. Winters, Nucl. Sci. Eng. **78**, 110 (1981).
[40]B. J. Allen, J. W. Boldeman, and R. L. Macklin, Nucl. Sci. Eng. **82**. 230 (1982).
[41]J. H. Conrad, Ph.D. thesis, Universität Heidelberg, 1976 (unpublished).
[42]K. R. Cosner and J. W. Truran, Astrophys. Space Sci. **78**, 85 (1981).
[43]K. Yokoi, private communication.
[44]J. Audouze and J. W. Truran, Astrophys. J. **202**, 204 (1975).
[45]M. Arnould, Astron. Astrophys. **46**, 117 (1976).
[46]S. E. Woosley and W. M. Howard, Astrophys, J. Suppl. **36**, 285 (1978).
[47]D. D. Clayton, Astrophys. J. **224**, L93 (1978).
[48]R. A. Ward and H. Beer, Astron. Astrophys. **103**, 189 (1981).
[49]H. Beer, F. Käppeler, K. Yokoi, and K. Takahashi, Astrophys. J. **228**, 388 (1984).
[50]F. Käppeler, K. Wisshak, R. R. Winters, G. Reffo, and A. Mengoni, in *Proceedings of the International Conference on Nuclear Physics, Florence, 1983* (Tipografia Compositori, Bo-

logna, Italy, 1983).
[51]M. J. Harris, Astrophys. Space Sci. **77**, 357 (1981).
[52]R. L. Macklin, J. H. Gibbons, and T. Inada, Nature (London) **197**, 369 (1963).
[53]*Table of Isotopes,* 7th ed., edited by C. M. Lederer and V. S. Shirley (Wiley, New York, 1978).
[54]B. J. Allen, G. C. Lowenthal, J. W. Boldeman, and J. R. de Laeter, in *Proceedings of the Fourth International Conference on Neutron Capture Gamma-Ray Spectroscopy and Related Topics, Grenoble,* IOP Conf. Series No. 62 (Institute of Physics and Physical Society, London, 1981), p. 573.
[55]D. D. Clayton, Astrophys. J. **139**, 637 (1964).
[56]W. A. Fowler, in *Cosmology, Fusion and Other Matters,* edited by F. Reines (University of Colorado, Boulder, 1972), p. 67.
[57]F.-K. Thielemann, J. Metzinger, and H. V. Klapdor, Z. Phys. A **309**, 301 (1983).
[58]F.-K. Thielemann, in Proceedings of the 2nd Workshop on Nuclear Astrophysics, Ringberg Castle, 1983, Max Planck Institut für Physik und Astrophysik, München, Report MPA 90; see also W. A. Fowler, Rev. Mod. Phys. **56**, 149 (1984).